

# DAMAGE-FREE REINFORCED CONCRETE BUILDINGS WITH GOOD REPAIRABILITY

Kazushi Shimazaki

*Professor, Dept. of Architecture and Building Engineering, Kanagawa University, JAPAN*

*Email: [shimazaki@kanagawa-u.ac.jp](mailto:shimazaki@kanagawa-u.ac.jp)*

**Abstract:** Recently, owners of buildings wish to continue using their buildings with low repair cost even after a severe earthquake. To achieve this, it is necessary to reduce the damage or to ensure good repairability of members. A building system consisted with “coupled shear core walls with damper” and flat plate slabs is one of the buildings having an ability of such demand. In this structural system, a large part of the horizontal force is resisted by the core wall, and most of the energy of the earthquake is absorbed in parts such as the boundary beam damper connected to the core walls. Repairability of these members is one of the most important factors in order to reuse the building. This paper examines the behavior of these members with de-bonded diagonal reinforcements to reduce the damage and so ensure good repairability.

## 1. INTRODUCTION

The goal of earthquake resistant design in any country is to protect life in very severe earthquakes by providing buildings with the strength and durability required to resist collapse. After a severe earthquake such as the Great Hanshin Earthquake, however, the demands of building owners changed: they want to be able to use the buildings again, at a low repair cost. In response, damage control design has recently become popular. This requires good repairability even for RC members to improve the performance of the member. On the other hand, the performance requirements of buildings during planning are diverse, such as improved habitability and large open spaces for flexibility. The structural system combined with RC core walls connected by damper beams and flat plate slabs as shown in Figure 1 is one structural type which meets these performance requirements.

In this structural system, a large part of the horizontal force is resisted by the core wall, and most of the energy of the earthquake is absorbed in parts such as the boundary beam damper connected to the core walls. To satisfy the ductility demand of the beams, diagonal reinforcements have been used [1]. Many experimental studies were carried out on using diagonal reinforced beams as members of a tube structure [e.g. 2, 3]. Although these beams showed very ductile behavior, the number of concrete cracks was quite large and damage to the beams prevented repair work. In those beams, the diagonal reinforcements yielded on the tension side only because concrete struts work with them on the compression side. This increases the number of concrete cracks, and increases the beam length. Repair work is thus laborious.

On the other hand, as a large part of the horizontal force is to be resisted in the core walls, severe shear force and

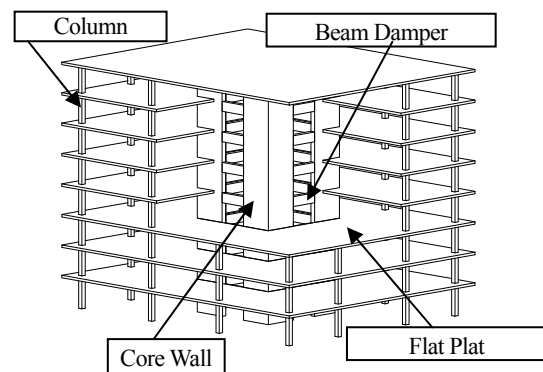


Figure 1 Prototype Building

bending moment act at the bottom of the walls. Diagonal cracks caused by this shear force reduce the shear stiffness of the core wall substantially. As shear stiffness cannot be restored by repair works, it is desirable to minimize such diagonal cracks. The horizontal cracks caused by bending moment will be closed by the action of the dead load after an earthquake; this damage, unless severe, is acceptable.

To improve the performance of the earthquake resistant wall, a 45-degree arrangement of bars, the combination of precast and pre-stressed, and removal of the bond of the main reinforcement of the wall and so on have been proposed[Sittipunt et al. 2000, Yahya et al. 2002, FIB 2003]. The objectives of these proposals were to ensure good ductile capacity, not to reduce the damage.

In order to reduce the damage of the structural system shown in figure 1, this study tested the damage reduction type boundary beams and earthquake resistant walls having de-bonded diagonal reinforcing bars which are expected to act as a brace.

## 2. De-Bonded Diagonally Reinforced Beam

### 2.1 Test specimens

The dimensions of the specimens are shown in Figure 2. All beams had eight diagonal reinforcement bars with four longitudinal reinforcement bars and web reinforcements. The section is 200 mm thick, 400 mm high and 1000 mm long. The overall length of the specimen is 2800 mm with end stubs of 400 mm thick, 1400 mm high and 900 mm long at both ends. These dimensions are one-third scale of the prototype structure shown in Figure 1. The specimens are divided into two series, one nominal and the other progressive.

The first of the series is summarized in Table 1. The primary experimental parameter is the bond of diagonal reinforcements, the second is the amount of web reinforcement, and the third is the strength ratio of rebar and concrete. Specimens #N-1 and #N-2 are common diagonal reinforcement beams, and specimens #N-3 to #N-8 are beams with de-bonded diagonal reinforcements. The amount of web reinforcement provided for #N-1 and #N-3 is consistent with the current AIJ standard [4, experimental equation]. For #N-2 and #N-4, the amount is calculated according to the AIJ design guidelines [5, truss model equation] with  $R = 1/50$  inelastic rotational ability. For #N-5, 6, 7 and 8, the amount at both end parts is doubled. The concrete compressive strength and the yield stress of the reinforcements are summarized in Table 1.

The other series (I series) is summarized in Table 2. These are improved ones having small notches near the beam end to reduce concrete cracks and thus improve repairability. Specimen #I-1 has 4-D16 parallel reinforcements anchored into the stub and the others have 2-D10 parallel reinforcements without anchoring into the stub. The notches are at the beam-end for specimen #I-1, and at 150 mm inside from the beam-end for specimens #I-2 through 6. All diagonal reinforcements are de-bonded. The amount of web reinforcement of #I-1 is the same as in #N-1 and 3, and the others are the same as in #N-5 to 8. The concrete compressive strength and the yield stress of the reinforcements are summarized in Table 2. Specimens #I-1, 2, 4, and 5 have axial reinforcements to deduce axial elongation. #I-1 and 2 are with bond and #I-4 and 5 are without. To create de-bonded reinforcement bars, wax and de-bond material (butylene rubber) were used for the deformed bars.

Loading cycles were applied to increase drift angle  $R$  with 3 repeated cycles. Only at the level of  $R = 1/100$  was the loading cycle conducted with 6 repeated cycles. These were determined by dynamic response analysis for the prototype building shown in Figure 1 during a severe earthquake to satisfy the energy dissipation ability. Specimens #6 and #8 were repaired after at the level of the  $R = 1/100$  cycle for #6, and  $1/67$  for #8. Then they were reloaded from the level of  $R = 1/200$ .

### 2.2 Experimental Results

During the response in the  $R = 1/700$  cycle, bending cracks were observed for all specimens at beam-ends. In the

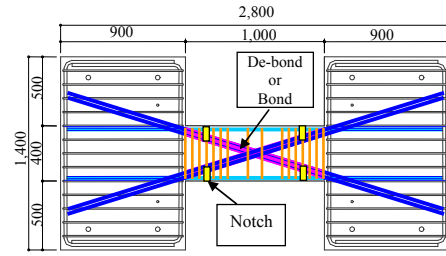


Figure 2: Dimensions of Test Specimens

Table 1 : List of the first series' specimens

Specimen	No. N-1	No. N-2	No. N-3	No. N-4	No. N-5	No. N-6	No. N-7	No. N-8
Section								
b×D(mm)	200×400							
Concrete (N/mm <sup>2</sup> )	54	51	54	51	51	64	48	32
Parallel Bars	2-D16							
σ <sub>c</sub> (N/mm <sup>2</sup> )	476	459	476	459		432	456	
X Shape bars	4-D16 Bond		4-D16 De-bond			4-φ 16 De-bond	4-φ 19 De-bond	4-φ 16 De-bond
σ <sub>s</sub> (N/mm <sup>2</sup> )	476	459	476	459		386	380	383
Web bars	2-D6 @150		2-D6 @100		2-D6 @100		2-D6 @100/@50	
σ <sub>s</sub> (N/mm <sup>2</sup> )	331	337	331	337		308	349	
p <sub>s</sub> (%)	0.21	0.32	0.21	0.32	0.32/0.64			
Tested year	2000	2001	2000	2001		2002	2003	

Table 2 : List of the I series' specimens

Specimen	No. I-1	No. I-2	No. I-3	No. I-4	No. I-5	No. I-6
Section						
b×D(mm)	200×400					
Concrete(N/mm <sup>2</sup> )	54	64	64	49	33	33
Parallel Bars	2-D16					
σ <sub>c</sub> (N/mm <sup>2</sup> )	476	370		380		
Axial bars	4-D16 Bond		2-D16 Bond	2-φ 19 De-bond		-
σ <sub>s</sub> (N/mm <sup>2</sup> )	476	849	380			
X Shape	4-D16 Bond		4-φ 19 De-bond			
σ <sub>s</sub> (N/mm <sup>2</sup> )	476	386	380			
Web	2-D6 @150		2-D6 @100/@50			
σ <sub>s</sub> (N/mm <sup>2</sup> )	331	308	349			
p <sub>s</sub> (%)	0.21	0.32/0.64				
Tested year	2000	2002		2003		

$R = 1/400$  cycle, bending-shear cracks were observed for the nominal series specimens. Diagonal shear cracks occurred at the center in the  $R = 1/100$  cycle except in specimens # N-3 and 6. For the specimens with de-bonded diagonal reinforcements (#N-3-8), cracks concentrated on both edge parts and the number of cracks was small. For the I-series specimens, a very small number of cracks concentrated on both edge parts with no shear crack at the center until large deformation occurred, except in #I-1. Crack patterns in the  $R = 1/100$  are shown in Figure 3.

The load-deflection behavior of the specimens are shown in Figure 4. Significant differences were not observed between the hysteretic response of the specimens until the  $R = 1/40$  cycle for N-series specimens. During the response in the  $R = 1/40$  cycle, strength degradation was observed due to shear yield for specimen #N-1, of diagonal reinforcements buckling at the center in negative loading for specimen #N-2, of bond failure for specimen #N-3, and of diagonal shear slip at the end for specimen #N-4. No degradation was observed for specimens #N-5, 6, 7, and 8.

For I-series specimens, the load-deflection curves are fat, and energy dissipation ability is larger than in the N-series specimens, except in #I-1. Specimens #I-2, 4, and 5

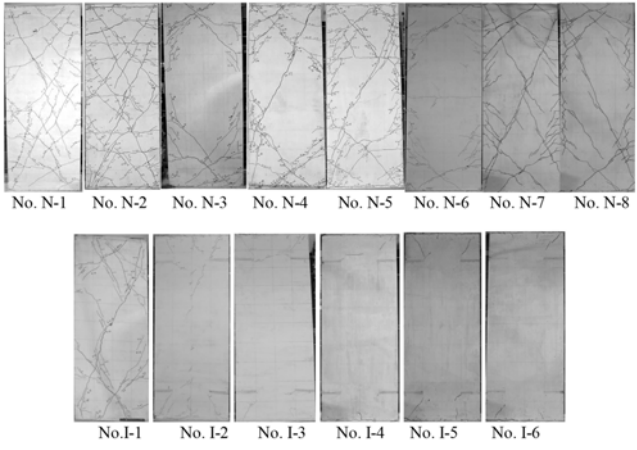


**Figure 3 : Crack Patterns ( $R=1/100$ )**

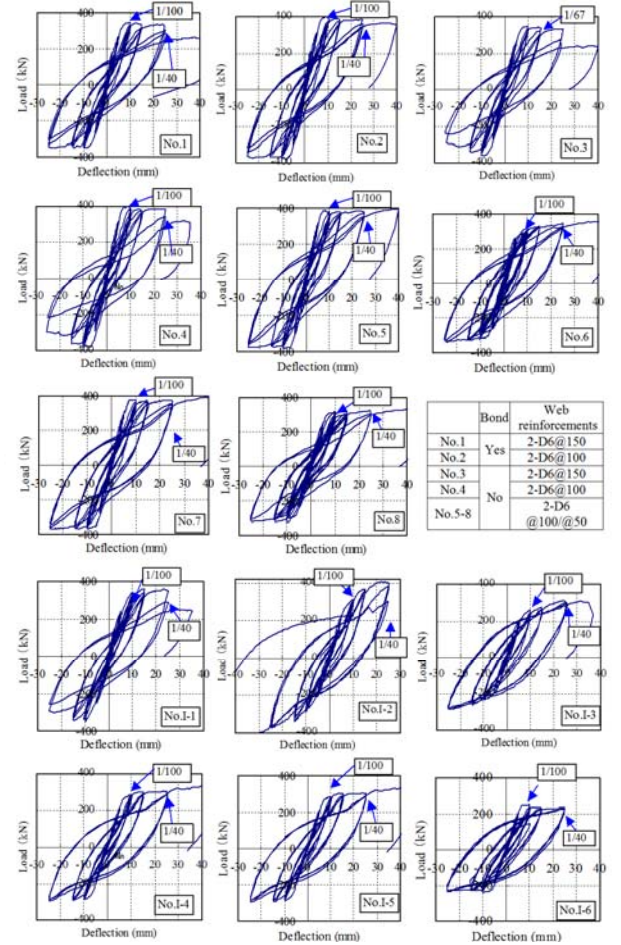
have pinching phenomenon at the occurrence of large deformation after  $R = 1/67$ . This seems to be caused by the axial bars that work as bending bars. In the relation of #I-2 at the second  $R = 1/40$  cycle, the load dropped because one of the X bars fractured at the welded part. These bars of specimens #I-2 and 3 were quench-hardened for strengthening, and weldability was not good.

Figure 5 shows the change of deformation components of bending deformation and shear deformation. The shear deformation part increases with increasing total deformation caused by shear cracks. Specimen #N-1 had large shear cracks in the center part, so the shear deformation part becomes much larger than that of the other specimens with slight cracking in the center. As specimen #N-6 had no shear cracks during the  $R = 1/100$  cycles, shear deformation is the smallest of the N-series specimens. Specimens of I-series had no shear cracks even at the occurrence of large deformation, except #I-1, so that shear deformation is minimal.

Figure 6 shows the equivalent damping factor of each specimen calculated from the first half cycle of the applied load – total deflection relationship shown in Figure 4. Significant differences were not observed in the equivalent damping factor between all N-series specimens. This means that the energy dissipation ability is the same, despite the clear difference of crack patterns shown in Figure 3 caused by the presence or absence of bond of the diagonal reinforcements. For I-series specimens, the equivalent damping factor becomes large compared with the N-series' value after the  $R = 1/100$  cycle. For the #I-2 specimen, the value was reduced because bond cracks of the axial reinforcements developed and stiffness degrading near zero load occurred as shown in Figure 4.

**2.3 Macro model and damage evaluation**

To evaluate the load resisting system and the condition of whether or not shear cracks developed at the central part, the load-carrying model was investigated as shown in Figure 7. A beam is divided into two systems, one diagonal steel bar truss system with concrete strut and the other a parallel-reinforced beam. As the tension force and the compression force should be equal for both the diagonal



**Figure 4 : Load-Deflection Curves**

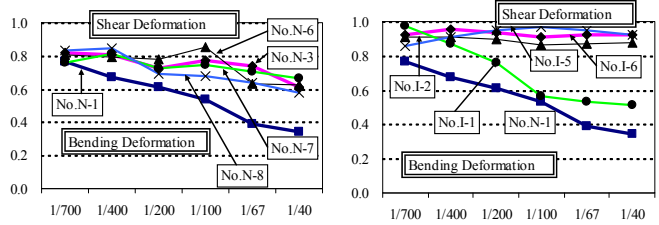


**Figure 5: Changing of deformation component**

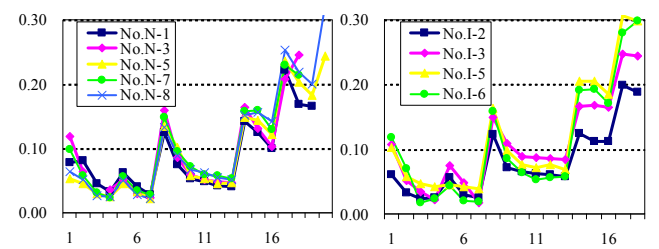


**Figure 6: Fluctuations in equivalent damping factor**

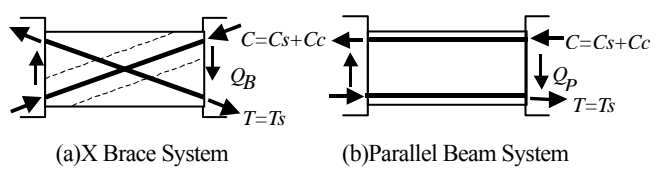


**Figure 7 : Macro model**

truss system and the parallel beam system, the compression force of concrete struts can be evaluated from the difference of force of the diagonal steel bar estimated from strain gage data. The ratio of  $C_s/T_s$  is shown in Figure 8(a)(b) for specimens #N-5, 6, 7 and 8 at the  $R = 1/400$  and  $1/200$  cycles. These values are almost constant despite the difference of concrete strength or yield strength of the steel bars. It is about 0.15 for the X brace system and 0.35 for the parallel beam system.

For the parallel reinforcement beam, the compression stress of concrete was calculated by elastic beam theory using steel bar force ( $T_s$ ) estimated from strain data. The area of compression was assumed from extreme compression fiber to neutral axis calculated from strain data of steel bars. According to the elastic beam theory, there is no compression stress of concrete in the middle part of the beam. Figure 8(c) shows the depth of compression area for specimens #N-5, 6, 7 and 8 at the  $R = 1/400$  and  $1/200$  cycles. In this figure, the calculated values using the elastic beam theory for the parallel beam section are also plotted. These values are also almost constant, and are about 0.2 times the total depth. This compression area is used for the brace system to obtain the compression stress of concrete struts. Shear force for concrete was calculated by subtracting the vertical force of the diagonal steel bar ( $T_s+C_s$  in Figure 7(a)) from the total shear force. Maximum shear stress of concrete is calculated as 1.5 times the mean shear stress for the all-rectangular section.

Using horizontal component of compression stress, tension stress by Poisson's effect ( $\nu = 1/6$ ), and shear stress,

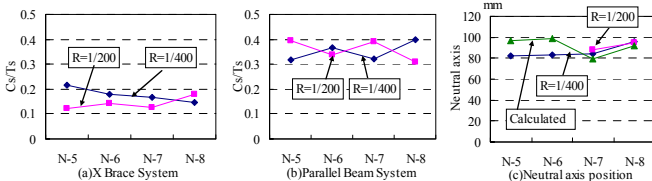
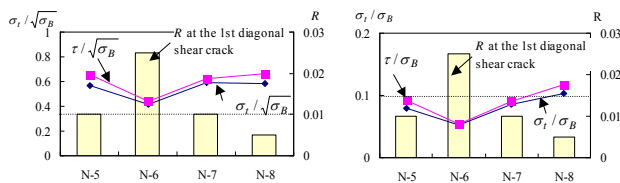


Figure 8 : Ratio of compression force to tension force



(a) Ratio to squirt of concrete strength (b) Ratio to concrete strength

Figure 9 : Ratio of tension stress

Table 3: Test specimens

Specimen	WP1	WX1	WSX1	WSX2	WTX1	WTX2
b × D (mm)	Main Panel		120 × 900		350 × 120	
	Orthogonal					
$\sigma_B$ (N/mm <sup>2</sup> )	44		43		43	
Vertical bars	End	6-D13 ( $\sigma_y=371\text{N/mm}^2$ )	6-D6 ( $\sigma_y=368\text{N/mm}^2$ )	12-D13 ( $\sigma_y=390\text{N/mm}^2$ )	14-D13 ( $\sigma_y=368\text{N/mm}^2$ )	
	Center	14-D13 ( $\sigma_y=371\text{N/mm}^2$ )		14-D13 ( $\sigma_y=368\text{N/mm}^2$ )	6-D6 ( $\sigma_y=374\text{N/mm}^2$ )	4-D6, 2-D16
	Orthogonal				8-D16 ( $\sigma_y=388\text{N/mm}^2$ )、6-D6	
Diagonal bars	12-D13 ( $\sigma_y=371\text{N/mm}^2$ )		12-D13 ( $\sigma_y=376\text{N/mm}^2$ )		12-D13 ( $\sigma_y=376\text{N/mm}^2$ )	
Horizontal bars	2-D10@70 ( $\sigma_y=387\text{N/mm}^2$ )		2-D10@70 ( $\sigma_y=353\text{N/mm}^2$ )		2-D10@70 ( $\sigma_y=353\text{N/mm}^2$ )	
Confining bars	Upper	2-D6@70 ( $\sigma_y=368\text{N/mm}^2$ )		2-D6@70 ( $\sigma_y=374\text{N/mm}^2$ )		2-D6@70 ( $\sigma_y=374\text{N/mm}^2$ )
	Lower					2-D6@35 ( $\sigma_y=374\text{N/mm}^2$ )

the principal tension stress is calculated by Mohr's circle. Figure 9 shows the calculated results at the calculated maximum load as the ratio to the square root of concrete strength in Figure 9(a), and to the concrete strength in Figure 9(b). Shear stress is also plotted in the same figure. The principal stress and the shear stress are almost the same. The specimens having large tension stress had the diagonal shear crack at an early load cycle. It seems that this model shows good agreement for examining the load-carrying system. I-series specimens have no compression concrete strut because of the notch. Therefore, as steel bars carry almost all of the shear force, the tension stress of concrete becomes nearly zero. The test results showed no diagonal shear crack.

### 3. Shear Walls with De-bonded Diagonal Reinforcements

#### 3.1 Test specimens

Six wall specimens of 1800 mm height, 900 mm width and 120 mm thickness were tested. They were part of the lower 2.5 stories of the prototype building shown in Figure 1. Following a preliminary analysis, the top of the specimen is at the height of the point of contraflexure of the first story core wall. The section arrangements of bars are shown in Table 3 and Figure 10.

WP1 is a common parallel reinforced wall. WX1 has de-bonded diagonal reinforcements arranged instead of the edge vertical reinforcing bars of 6-D13 of WP1, and additional 6-D6 were arranged at that place for confining bars. WSX1 was divided at each story assuming a precast panel, and WSX2 has crack generation plates of 0.6-mm thickness which divide the panel horizontally into three parts. Each gap between the panels was filled with grout mortar. The edge vertical reinforcement of both WSX1 and WSX2 was de-bonded and fixed at the panel boundary by fixing plates of 40x40x6 mm and nuts. The other reinforcements in the panel were the closed type and were anchored in it. WTX1 is a T-shape specimen with an orthogonal wall for concentration of the L type flange wall. WTX2 has D16 reinforcing bars instead of D6 at the other end of the flange wall (hereafter called "free end"). The bar is cut off at 160 mm in the lower stub, and de-bonded in the stub. This is expected to increase the compressive strength at the free end and not increase the tensile strength. The former prevents concrete crushing caused by the large tensile strength of the orthogonal wall, and the latter prevents an increase in the number of cracks.

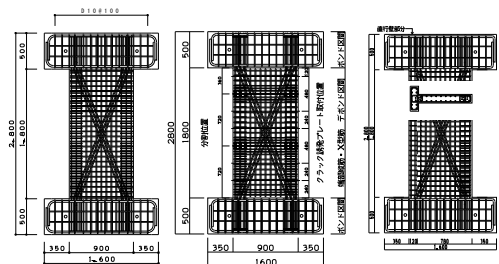


Figure 10: Section arrangements of bar

Cyclic horizontal force is applied at the top of the wall under constant axial compression load of 392 kN for the plane type walls, and 490 kN for the T shape walls ( $\sigma_0 = 3.6 \text{ N/mm}^2$ ). The loading cycle is one cycle at  $R = 1/700$ , three at  $R = 1/400$  and  $1/200$ , six at  $R = 1/100$ , three at  $R = 1/67$ , and finally one way loading to  $R = 1/33$ .

### 3.2 Experimental results

Crack patterns at  $R = 1/200$  and  $1/100$  of each test specimen are shown in Figure 11. Bending cracks occurred in the cycle at  $R = 1/700$  for all test specimens. Bending shear cracks occurred at  $R = 1/400$  for WP1, WTX1 and WTX2, and at  $R = 1/200$  for WX1.

At  $R = 1/200$ , the diagonal bending shear crack was conspicuous for WP1, whereas for WX1, the horizontal crack region was wide and there were few diagonal shear cracks. For WTX1 and WTX2, when the orthogonal wall side became compressed, horizontal cracks were observed in the tension side but when the orthogonal wall side became tension, only diagonal cracks were observed. Also, few diagonal cracks were observed in WSX1 and WSX2.

At  $R = 1/100$ , signs of concrete crushing in the bottom part were observed for WP1, WX1, WSX1 and WSX2. The maximum crack width except at the bottom boundary was 0.2 mm for WP1, and 0.05 mm for WX1. For WTX1, the edge D6 reinforcing bars buckled and fractured during repeating loading. The concrete crushing region expanded to the central part with increasing damage to the edge. For WTX2, concrete crushing stayed in the concrete surface. For WSX1 and WSX2, the diagonal cracks decreased substantially compared with WX1. The remaining crack width at the bottom boundary of the wall panel was about 0.4 mm for both WSX1 and WSX2.

At  $R = 1/67$ , for WTX1, the concrete crushing progressed in both end parts, and for WTX2, it progressed into the center part. At  $R = 1/33$ , the concrete crushed part progressed in both end parts for WP1, WX1, WSX1 and WSX2, however the axial load was maintained until the last cycle. Hence, the deformation capacity is sufficient.

The relationships of horizontal force and top displacement of the specimens are shown in Figure 12. For all specimens except the T-shape model, the maximum load was maintained until at  $R = 1/67$ , after which the strength declined gradually. For WX1, the vertical reinforcement of D6 in the edge part buckled at  $R = 1/40$  and the strength declined. For WTX1, after the strength declined at  $R = 1/100$ , concrete was crushed in the compression side, and D6 reinforcements broke. Then, the cycle was reduced once at  $R = 1/67$ , and additional one-way loading for the orthogonal wall compression side was performed until  $R = 1/40$ . For WTX2, the control displacement of the first cycle at  $R = 1/67$  exceeded the target value caused by range-over of the control displacement gauge and the data could not be obtained. The gray line in the figure is the value estimated from the test minute. At  $R = 1/100$  cycle, even concrete was crushed in the unconfined region, the strength kept the maximum value, and the strength declined at  $R = 1/67$  caused by buckling of D13 rebars. In the figure, the solid

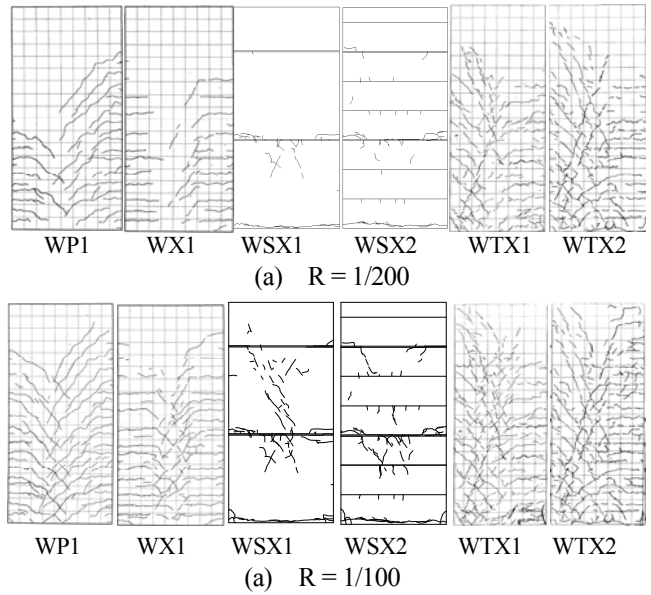


Figure 11: Crack pattern

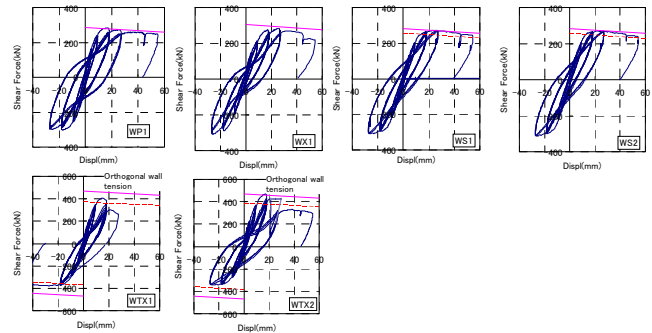


Figure 12 : Relationships of horizontal force and top

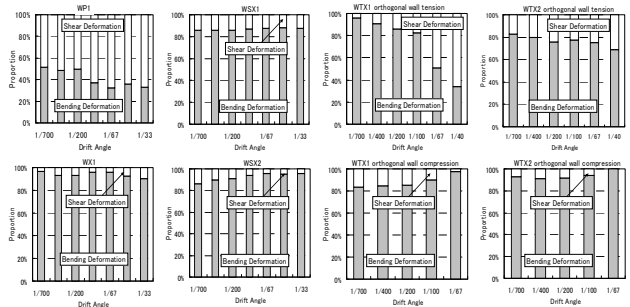


Figure 13 : Bending and shear deformation

and dashed lines are calculated values.

The calculated value, which is the sum of the shear force at the full plastic moment of parallel reinforcements and the yield strength of the horizontal components of the diagonal reinforcements, is shown by the solid line in Figure 12. The line was modified with deflection by considering the P-Delta effect of the vertical load and the horizontal component of inclined vertical load. WP1 withstood the shear force at the full plastic moment until large deformation. The strength of WX1, WSX1 and WSX2 at large deformation was less than the calculated value. For WTX1 and WTX2, the test values were small compared with the calculated ones on the positive side where the orthogonal wall becomes a tension side. In the negative side where the

orthogonal wall becomes a compression side, the tested values were quite low.

The dashed line is the calculated load-deflection relations considering the strain distribution. The compression stress of X bars is assumed to be 1/4 of the yield stress for WSX1 and 1/2 for WSX2. The test results were higher than the calculated values until large deformation. For WTX1 and WTX2, because the de-bonded X bars do not work fully, the calculation values ignored the X bars. They showed good agreement with the test results.

Bending deformation was calculated by integrating the curve obtained from the piecewise axial displacement difference of both wall edges. Shear deformation was calculated by subtracting the bending deformation from the total horizontal deformation. Figure 13 shows the deformation components of bending and shear deformation at the peak point of each loading cycle. The shear deformation component accounts for over 50% of the total deformation for WP1 of the common parallel reinforcing type wall. For WX1 having the de-bonded X type reinforcing bars, the bending deformation component accounts for over 80% and increases with deformation except at the final stage. This corresponds to the phenomenon that the shear crack of WX1 decreases and that the bending crack stretches to the center part. For WSX1 in which the panel wall was divided in each story, the bending deformation component accounts for over 85%, and 90% for WSX2 in which panels divided the horizontal direction into three parts. For WTX1 with the orthogonal wall, the deformation component ratio is almost the same as the value of WX1 when the orthogonal wall is the compression side, in contrast with the tension side, and the shear deformation component becomes larger because of the large shear force caused by large bending strength. At large deformation, the compression concrete of the wall edge was crushed and slipped at the base boundary, and so the shear deformation component increased. In WTX2 which has heavy confining reinforcements in the compression area, the shear deformation component does not increase as much as WTX1, even in the case of large deformation.

Figure 14 shows the equivalent damping factor of each specimen. Over  $R = 1/100$ , as the X bars do not yield in the compression side, the load-deflection curve shows an inverted S shape, and the equivalent damping factor of WX1 is less than that of WP1. The values of WSX1 and WSX2 are approximately equal to WX1. The damage was substantially reduced compared with WX1 but having equal energy absorbing capacity. For WTX1 and WTX2, when the orthogonal wall is in the compression side, the value is slightly larger than the value of WX1. When the orthogonal wall is in the tension side, however, the value of WTX2 with heavy confining reinforcements in the compression area is smaller than that of WTX1 because of small damage.

#### 4. CONCLUSIONS

This paper examined the RC members with diagonal reinforcements to reduce damage during a severe earthquake for good reparability. The main findings are as follows:

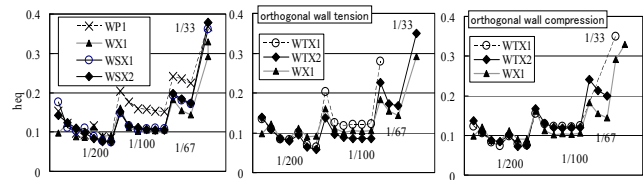


Figure 14 : Equivalent damping factor

1. The results of this experimental investigation demonstrated that de-bonded diagonal reinforcements are an effective means to reduce the number of cracks.
2. For the beams, the macro model showed good agreement with the tested results.
3. For shear walls, by forming a panel wall at each story and de-bonding the main vertical reinforcements in the panel, the bending deformation component increases with concentration in the panel boundary. As a result, shear cracks and bending cracks in the panel center do not occur, and so the wall has good reparability.
4. The horizontal strength of the wall can be calculated as the summation with shear strength of the parallel arrangement wall and the horizontal component of X bar brace yield strength with whole area of tension brace and a half area of compression brace in safe side until large deformation. The stress of concrete on the compression side becomes large because the compression X bars do not result in yielding. An adequate amount of confining reinforcement is necessary to secure deformability in the case of large deformation.

#### Acknowledgements:

This study was funded by Frontier Research Program of MEXT and Grants-in-Aid for Scientific Research of JSPS. The opinions and findings do not necessarily represent those of the sponsor.

#### References:

1. Park, R. and T. Paulay, Reinforced Concrete Structures, A WILEY-INTERSCIENCE PUBLICATION, 1975
2. Eto, H., K. Yoshioka, et al., Aseismic design of 41 story reinforced concrete tube structure –Part 4 Ultimate shear strength of short beams-, Summaries of technical papers of annual meeting, C, Architectural Institute of Japan, 1989, pp.773-774 (In Japanese)
3. Shimazaki, K. and Y. Hayakawa, Experimental study for ductility of short beams, Proceedings of the Japan Concrete Institute, 1990, pp.179-184 (In Japanese)
4. AIJ, AIJ Standard for structural Calculation of Reinforced concrete Structures –Based on Allowable Stress Concept–, Architectural Institute of Japan, 1999.
5. AIJ, Design Guidelines for Earthquake Resistant Reinforced Concrete Buildings Based on Inelastic Displacement Concept, Architectural Institute of Japan, 1999.
6. Sittipunt, C. and wood, S. L. (2000). Development of reinforcement details to improve the cyclic response of slender structural walls, 12th World Conference on Earthquake Engineering, Paper 1770.
7. Yahya, C., Kurama, Y., Sause, R., Pessiki, S., and Lu, L.W. (2002). Seismic Response Evaluation of Unbonded Post-Tensioned Precast Walls, ACI Structural Journal, Vol. 99, No. 5, pp. 641-651
8. FIB (2003). Seismic design of precast concrete buildings, state of art report, fib bulletin, No.27